coatings

MDPI

Review

Optical Antireflective Films: Single-Scale Limits, Cross-Scale Synergy, and Evidence-Based Application Mapping

Shunyao Zhang [1], Enming Zhao [2] and Shuangqiang Liu [1,3,*]

[1] School of Physics and Astronomy, Sun Yat-sen University, Zhuhai 519082, China; zhangshy268@mail2.sysu.edu.cn
[2] School of Engineering, Dali University, Dali 671003, China; zhaoem163@163.com
[3] Guangdong Provincial Key Laboratory of Quantum Metrology and Sensing, Sun Yat-sen University, Zhuhai 519082, China
* Correspondence: liushq33@mail.sysu.edu.cn

Abstract

Optical antireflective films regulate interfacial reflection and improve light utilization in optical and optoelectronic devices. Interference-based thin films, micron-scale textures, and nanostructures each have distinct performance limits. Combining these architectures alone does not establish cross-scale synergy. This review distinguishes single-scale advantages, cross-scale composites, and evidence-supported cross-scale synergy. It evaluates the evidence using control level, metric hierarchy, reporting completeness, the four synergy criteria, and a separate translation-readiness tier. The four synergy criteria are functional separation, a matched single-scale control, repeatable device-level gain, and scale-coupling evidence. The translation-readiness tier separately assesses manufacturing and reliability evidence. Among the studies included in this review, none met all four synergy criteria. The reviewed composites therefore remain cross-scale composites rather than demonstrated cross-scale synergies. Matched controls, scale-coupling evidence, failure cases, scalable manufacturing, and long-term reliability remain the principal gaps.

Keywords: antireflective coatings; interference thin films; micro/nanostructures; cross-scale synergy; matched controls

1. Introduction

When light crosses an interface between media, the optical boundary determines how incident energy is distributed among transmission, reflection, and absorption. According to the Fresnel equations, a polished glass surface with a refractive index of 1.5 reflects about 4% of normally incident light, whereas a high-refractive-index semiconductor such as silicon ($n \approx 3.5$) can exhibit a single-interface reflectance above 30% [1]. Cumulative losses from multiple untreated interfaces substantially reduce the total transmittance of an optical system [2]. Antireflective coatings therefore affect optical efficiency, image contrast, detector sensitivity, thermal management, and long-term system reliability.

Antireflection requirements vary by application. For example, photovoltaic devices need to maintain low reflectance across the solar spectrum and wide incidence angles, while industrial-grade crystalline silicon solar cells typically need to reduce reflectance below 10%. Porous silicon and nanostructures can further reduce reflectance; for example, double-layer porous silicon has a reflectance below 3% in the 400–1000 nm wavelength range [2]. High-power laser systems require ultra-low reflectance and a high laser-induced damage threshold (LIDT), with some designs requiring average transmittance above 99% [3].

Check for updates

Academic Editor: Luigi Calabrese

Received: 30 September 2026
Revised: 22 October 2026
Accepted: 23 October 2026
Published: 26 October 2026

Copyright: © 2026 by the authors. Licensee MDPI, Basel, Switzerland. This article is an open access article distributed under the terms and conditions of the Creative Commons Attribution (CC BY) license.

Infrared imaging windows require simultaneous reduction of reflection from mid-wave infrared (MWIR, 3–5 μm) and long-wave infrared (LWIR, 8–14 μm) [4]. Displays, such as liquid crystal displays (LCDs) and cathode-ray tube monitors (CRTs), automotive systems, and photovoltaics require broadband antireflection, environmental stability, and self-cleaning or hydrophobic functions. Environmental stability includes mechanical durability and thermal stability. Processes such as magnetron sputtering can achieve large-area uniform coatings [5]. Systematic reviews have already examined the materials, design, and performance evaluation of photovoltaic antireflective films [6]. Augmented reality/virtual reality (AR/VR) displays have also driven specialized research into low-reflectance, low-polarization optical materials [7].

Interference thin films are currently the most industrialized solution. Their optical response is determined by phase-controlled multibeam interference and can be calculated using the transfer-matrix method [1]. To achieve broader spectral and angular responses, thin-film designs have evolved from single-layer films to bilayer V-shaped (or W-shaped) and multilayer films, such as alternating SiO_2/TiO_2 structures. Fabrication processes such as magnetron sputtering, electron beam evaporation, and plasma-enhanced chemical vapor deposition (PECVD) can control nanoscale thickness [5] and support large-scale production or precision manufacturing [8]. Material selection remains the main limitation on interference-film performance. Magnesium fluoride (MgF_2, n = 1.38) is often used as the low-index layer, whereas high-index substrates such as silicon have a refractive index above 3.4. This large index difference makes it difficult to form a continuous transition from air (n = 1) to the substrate [2]. When the available refractive index is limited, inverse design can produce antireflective structures that achieve near-perfect transmission through complex media [9]. However, interference is wavelength-sensitive, and the laser-induced damage threshold (LIDT) is affected by film defects and interfacial stress [10]. Reduced adhesion in multilayer films can also cause interfacial delamination or mechanical failure, requiring process-specific control [5].

Surface engineering takes a different approach by directly modifying interface morphology. Micron-scale geometries reduce reflection through multiple reflections, refraction, and optical path extension, and they can enhance absorption in the active layer. For example, micron-scale pyramid structures (SiMPs) increase absorption [11]. These structures are integrated with the substrate, reducing adhesion problems and thermal mismatch in thin-film systems. Wet etching is now the standard texturing process for crystalline silicon photovoltaics [2]. However, light trapping weakens at extreme incidence angles, and the increased surface area promotes carrier recombination in active devices [11].

Nanoscale structures operate mainly through wave optics. Subwavelength gratings, porous layers, and moth-eye structures can form effective refractive-index gradients, enhancing light coupling into the substrate or extending the optical path in the thin-film absorber [12]. These mechanisms can improve broadband and wide-angle performance, but high-aspect-ratio structures are prone to wear and contamination and increase surface recombination in devices. Resonant structures are limited by bandwidth and angular stability [13]. Early biomimetic silicon nanostructures already exhibited broadband, quasi-omnidirectional antireflection [14], and patterned micro/nanostructure arrays have been used for light management in photovoltaics, optoelectronics, and optical devices [15].

Interference thin films, micron-scale geometries, and nanoscale wave-optical structures make different trade-offs in broadband performance, angular response, mechanical support, passivation, and electrical compatibility [16]. These differences motivate cross-scale design, but structural stacking alone does not establish synergy. The framework therefore addresses two questions. First, synergy identification requires four criteria: (i) functional separation across scales; (ii) a matched single-scale control under consistent materials, device structure,

and test conditions; (iii) repeatable device-level gain; and (iv) scale-coupling evidence. Scale coupling is verified only by an additive-model comparison, a scale-blocking, removal, or replacement experiment, or a direct measurement of cross-scale coupling. Second, translation readiness is assessed separately from synergy using manufacturing evidence (yield, cost, or defect density) and reliability evidence (lifetime, environmental stability, or failure boundary). A system that satisfies all four criteria is classified as cross-scale synergy, whereas one that also meets the readiness criteria is classified as translation-ready cross-scale synergy. Scale-coupling evidence is supported by work on multiscale hierarchical materials [17,18], cross-scale computational–experimental coupling [19], multiscale modeling [20], and multiscale photonic device characterization [21]. Engineering readiness is therefore not part of the physical definition of synergy.

Previous reviews have focused on antireflective materials [2,16], bioinspired nanostructures [12,13], photovoltaic light management [6,22], or specific fabrication methods [5,8]. The novelty of this review lies not in compiling another catalogue of materials. It lies in separating composite formation from scale coupling, separating physical synergy from translation readiness, and introducing a control-aware evidence map that combines A/B/C control grading, metric hierarchy, reporting completeness, and application-specific evidence boundaries. Table 1 compares this review with the prior review literature on these dimensions.

Table 1. Comparison of this review with prior antireflective-film reviews.

Prior Review	Primary Focus	Control Grading	Scale-Coupling Criterion	Translation Readiness	Application Mapping
Shanmugam et al. [2]	Photovoltaic (PV) antireflective materials	Not stated	Not stated	Not stated	PV context
Khan et al. [5]	Coating processes	Not stated	Not stated	Not stated	Broad applications
Ji et al. [6]	Solar-cell antireflection	Not stated	Not stated	Not stated	PV context
Butt et al. [8]	Thin-film fabrication	Not stated	Not stated	Not stated	Integrated photonics
Yang et al. [12]	Moth-eye nanostructures	Not stated	Not stated	Not stated	Broad optics
Han et al. [13]	Bioinspired materials	Not stated	Not stated	Not stated	Broad materials
Raut et al. [16]	Antireflective coatings	Not stated	Not stated	Not stated	Materials and design
Ali and Karasu [22]	PV antireflective technologies	Not stated	Not stated	Not stated	PV context
This review	Evidence appraisal across all routes	A/B/C plus completeness	Scale-coupling evidence	Separate readiness tier	Application-specific map

Table 1 note: full-text keyword checks were completed for all eight prior reviews [2,5,6,8,12,13,16,22]. None defines a control-grading framework, a scale-coupling criterion, or a translation-readiness tier.

Review Scope and Literature Selection

This review is a targeted narrative review rather than a systematic review [23]. The initial literature pool was identified using Google Scholar and cross-checked in Web of Science, Scopus, and ScienceDirect. The search combined terms related to antireflection coatings, photonic light management, surface texturing, gradient-index coatings, Mie

resonance, moth-eye structures, and applications in photovoltaics, infrared optics, and optoelectronic devices. Snowballing from foundational and highly relevant references was also used. The searches were conducted on 15 May 2026 and 18 September 2026, covering publications from 1950 to June 2026. The Boolean search combined antireflection coating (ARC) and light-management terms with application- and material-related terms. Studies were included when they addressed the optical mechanisms or applications under review, represented original physical principles or data, provided comparable experimental or theoretical results, or had clear citation visibility. The corpus was then stratified into mechanistic cases, direct comparative evidence, secondary summaries, and application cases. Screening identified 1860 records, reduced to 1290 after duplicate removal; 860 records were excluded after title/abstract screening. Of 430 full-text articles, 320 were excluded, leaving 110 core evidence records. Together with eight methodological and readiness references, the revised reference list contains 118 entries.

To avoid confusion among scale concepts, structures with feature sizes below 100 nm are classified here as nanoscale, those from 100 nm to 1 µm as submicron, and those from 1 to 100 µm as micron-scale. Continuous films are not assigned to a scale solely by thickness; when they perform an independent function through interference, admittance matching, or passivation, they are treated as functional layers distinct from structural scales. Figure 1 clarifies how layers are counted rather than defining the structural scale ranges themselves. Panel (a) distinguishes optically resolvable layers, whereas panel (b) distinguishes process- or function-defined layers. This distinction prevents a continuous film from being counted as an additional structural scale merely because it contains multiple optical sublayers. Device-level integration and evaluation are not structural scale domains. Cross-scale systems must therefore involve either two non-overlapping structural scale domains or coupling between a structural scale and an independent functional layer.

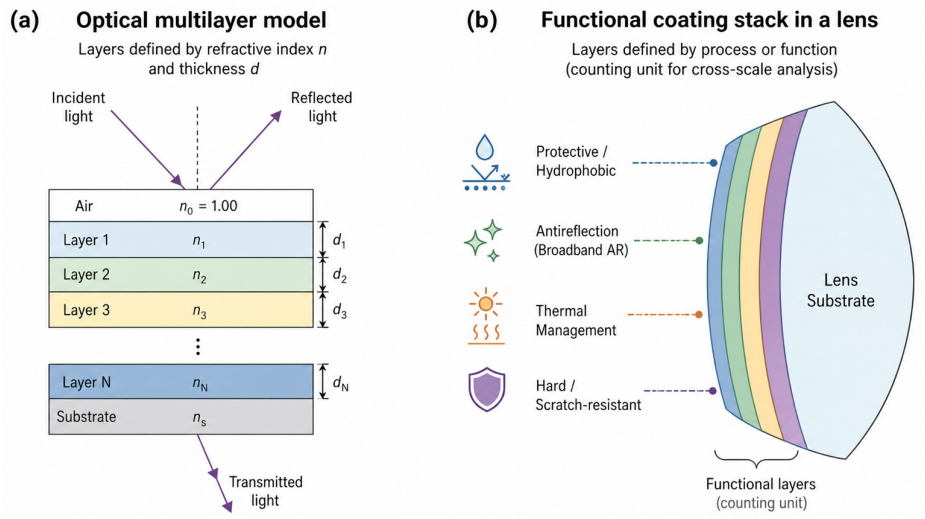


Figure 1. Layer definitions used in this review. (**a**) An optical multilayer model in which each layer is defined by a specific refractive index n and thickness d. (**b**) A functional coating stack in a lens, in which layers are defined by their process or function. For cross-scale counting, the functional layers in (**b**), rather than individual optical sublayers, provide the counting unit.

The A/B/C grades denote control level only. Grade A is a matched single-scale control from the same batch or device; Grade B is a comparable control within the same study but with incomplete information on batch, device, or test conditions; Grade C includes simulations, cross-study comparisons, or studies without a comparable single-scale control. The metric hierarchy comprises material, optical, and device levels. Reporting completeness requires core metrics, test conditions, sample size or replicates, and uncertainty. Missing

information is recorded as partial. Control level does not replace the separate assessment of the four synergy criteria and the translation-readiness tier.

The four synergy criteria are assessed as follows. Functional separation requires an independent measurement, blocking, removal, or replacement experiment; mechanism-only evidence is unverified. Matched controls prioritize the same batch or device, followed by same-study controls with consistent materials and test conditions. Device-level gain requires replication across samples, batches, or statistical units. Scale-coupling evidence requires an additive-model comparison, a scale-blocking/removal/replacement experiment, or a direct cross-scale coupling measurement; coexistence of functions is recorded as unverified. Translation readiness is assessed separately: manufacturing requires at least one of yield, cost, or defect density, and reliability requires at least one of lifetime, environmental stability, or a failure boundary. Translation readiness follows established technology-readiness and manufacturing-readiness concepts [24–26]. Figure 2 summarizes this two-tier framework.

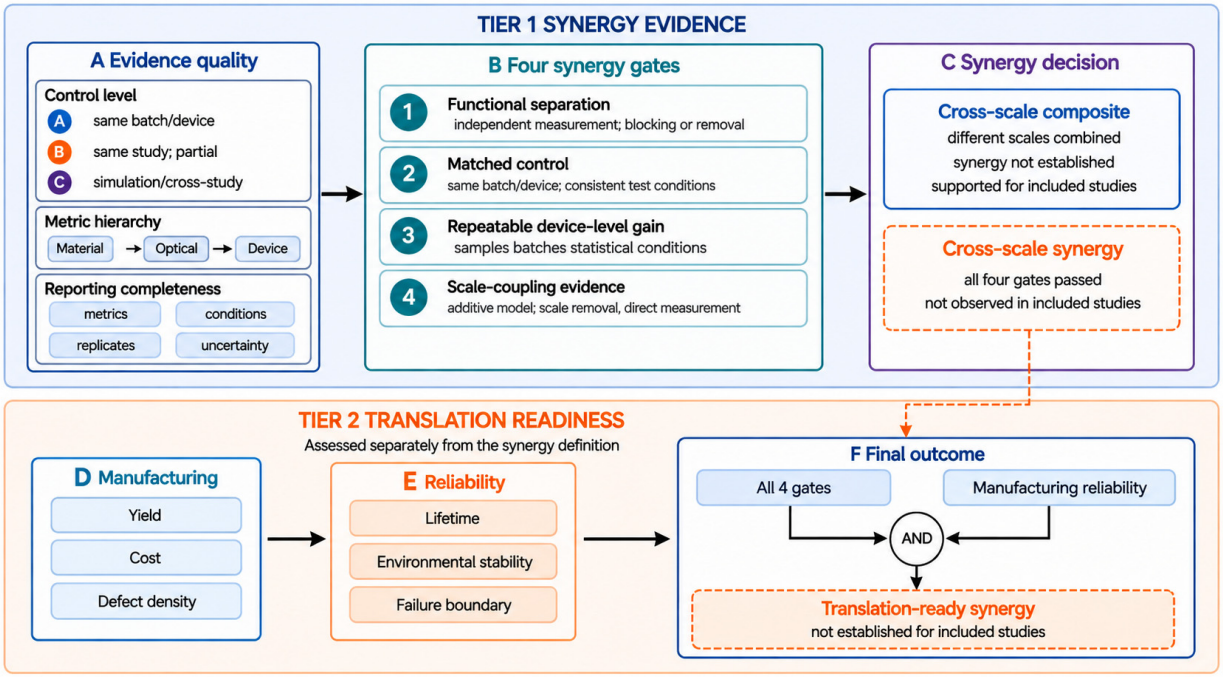


Figure 2. Two-tier decision framework. First, four synergy criteria are assessed: functional separation, matched single-scale control, repeatable device-level gain, and scale-coupling evidence. Second, translation readiness is assessed separately using manufacturing and reliability evidence. Cross-scale synergy is claimed only when all four synergy criteria are met. Translation-ready cross-scale synergy requires both synergy and readiness evidence. Arrows indicate the direction of assessment; colors distinguish panels only. Dashed orange out-lines and the dashed arrow denote outcomes not observed (Tier 1) or not established (Tier 2) among the studies included in this review.

2. Interference Thin Films: Established Technology and Performance Limits

This section establishes a single-scale baseline for the later cross-scale assessment by examining performance limits and failure mechanisms.

2.1. Physical Principles and Evolution of Multilayer Design

Interference-based antireflective films rely on interference cancellation between one or more interfacial reflections [1]. For single-layer uniform thin films, complete cancellation at the design wavelength requires matching amplitudes of the two reflected light beams, with phase differences of an odd multiple of π. The ideal film therefore has a refractive index

equal to the geometric mean of air and substrate refractive indices, with an optical thickness of one quarter of the design wavelength [1,27]. At oblique incidence, the effective optical thickness and reflection coefficient are polarization-dependent, so s-polarization and p-polarization must be considered separately. Fresnel's observations of thin film interference and subsequent research on optical thin films form the physical basis for modern multilayer film design [28].

The transfer-matrix method efficiently describes the optical response at arbitrary wavelengths and incidence angles [1]. Each layer is represented by a 2×2 matrix; multiplying the matrices of all layers yields the reflection and transmission amplitudes of the complete multilayer stack. This method provides a standard numerical framework for thin-film design and supports deterministic optimization. Tensor operations and automatic differentiation can now compute wavelength- and angle-dependent responses in parallel, reducing computation time and enabling multiparameter gradient optimization [29]. However, the transfer-matrix method cannot remove performance limits imposed by the available materials and phase conditions.

As designs evolved from single layers to V-shaped bilayers and broadband multilayers, complexity increased [16]. Under appropriate refractive-index and thickness conditions, a bilayer can suppress reflection at two discrete wavelengths; adding more layers produces flatter reflection spectra and provides additional degrees of freedom. Global optimization methods such as needle optimization, genetic algorithms, and memetic or mixed-integer programming can escape local minima and have been applied to stacks ranging from several layers to more than twenty layers. Generative and sequential machine-learning methods combined with global optimization, such as OptoGPT and GLOnet, can also determine materials, thicknesses, and layer numbers [30]. For example, deep-learning-assisted Ge/Al_2O_3 and Ge/SiO_2 multilayers in the 3–5 μm and 8–12 μm bands achieved a minimum average reflectance of 0.36 in the original finite-difference time-domain (FDTD) simulations. Because no percent sign or normalization was reported, this value is retained as originally stated [31]. These methods improve design efficiency but do not change the accessible refractive-index range, material absorption, or angular sensitivity of interference. Algorithmic advances therefore do not alter the fundamental physical limits of planar thin films.

Graded-index designs represent the limiting form of multilayer films, in which the refractive index varies continuously from the substrate to air [32]. Such structures can reduce reflection over broad spectral and angular ranges and mitigate scattering and stress concentration caused by sharp interfaces [33]. In practice, alternating high- and low-index layers with thicknesses much smaller than the wavelength approximate a continuous gradient. Yang et al. combined an 11-layer $SiO_2/Al_2O_3/TiO_2$ stack with a graded-index film and achieved average reflectance values of 0.72% from 420 to 2000 nm and 1.55% from 3000 to 5000 nm [34]. This approach is effective, but discrete approximations remain constrained by layer count, material dispersion, and fabrication errors, motivating later subwavelength and porous effective-medium structures [35].

2.2. Industrial Advantages and Performance Limits

Physical vapor deposition and chemical vapor deposition (PVD/CVD) have made interference thin films an established industrial technology. Magnetron sputtering, ion-assisted deposition, and plasma-enhanced chemical vapor deposition can control thickness, composition, and microstructure [3,36–38]. Design software and material databases can predict optical performance before fabrication [39]. Deposition processes can also be integrated with semiconductor and optical manufacturing lines [8]. Therefore, for lenses, windows,

filters, and photovoltaic devices with moderate spectral and angular requirements, planar interference thin films remain the default solution.

Interference thin films are used across multiple spectral bands. Bilayer or trilayer graded-index films, such as SiO_2/TiO_2 multilayers, can reduce visible reflectance below 1%, and additional surface layers can provide hydrophobicity or self-cleaning [5]. In photovoltaics, indium tin oxide and plasma-enhanced films are used for perovskite light management [40]. High-bandgap materials and ion-beam sputtering can improve the laser-induced damage threshold (LIDT) for laser and space optics. SiOxNy graded-index films have achieved an average transmittance of 99.01% and an LIDT of 7.15 J/cm^2 [3]. Dual-band coatings extend infrared applications [41], and quantum-dot-enhanced coatings can improve antireflection performance in photovoltaic devices [42]. When broadband, wide-angle, high-LIDT, and long-term stability requirements are combined, the limitations of interference coatings become more apparent.

Multibeam interference is highly sensitive to wavelength and incidence angle. Reflection minima shift with wavelength and angle, and even optimized designs struggle to maintain an average reflectance below 1% from normal incidence to 80° [43]. At oblique incidence, the effective optical thickness changes, the central wavelength shifts, and s- and p-polarized components separate; performance degrades markedly above approximately 60–70° [39]. This behavior is intrinsic to interference and cannot be eliminated solely by improving deposition accuracy.

Material selection also limits performance. Conventional natural optical materials cannot provide a continuous refractive-index transition from air to a high-refractive-index semiconductor, and many materials exhibit dispersion or absorption in the ultraviolet, visible, or infrared [16]. Graded films can approximate an ideal profile, but they require multilayer structures and strict control of material compatibility; the limited refractive-index contrast also constrains the maximum bandwidth achievable with a small number of layers.

Conformal coverage and interface reliability limit the long-term performance of interference thin films. Achieving uniform deposition on curved surfaces, flexible substrates, and high-aspect-ratio structures is difficult; for example, PVD has limited coverage of complex geometries [8]. In multilayer films, thermal expansion mismatch, interdiffusion, residual stress, and interfacial absorption reduce mechanical durability and lower the LIDT, as does the superposition of laser-induced thermal and interfacial stresses originating from defects [3,10]. Interfacial delamination or mechanical failure caused by reduced adhesion must still be controlled for each process [5]. High temperature, high humidity, ultraviolet (UV) irradiation, and thermal cycling may cause delamination, cracking, or spectral drift. In high-power laser and space applications, these failure modes are often more critical than initial reflectance.

Material, interference, and interface constraints together define the performance limits of planar thin films and have motivated a shift from material stacking toward cross-scale interface engineering. The next section compares the two single-scale surface-engineering routes, namely micron-scale and nanoscale structures, and their complementary limitations.

3. Single-Scale Surface Engineering: Geometric Optics and Wave Optics

Surface engineering controls reflection by modifying interface morphology and the local optical environment [44]. Micron-scale geometric light trapping is governed mainly by ray optics, whereas nanoscale subwavelength and resonant structures rely on effective-medium, scattering, diffraction, and resonance effects. The different mechanisms and failure modes of these routes provide a basis for subsequent cross-scale integration. Bioinspired micro/nanophotonic materials also offer design principles for coupling interface

morphology with optical function [45]. Figure 3 summarizes the benefits and conditional risks of three single-scale mechanisms.

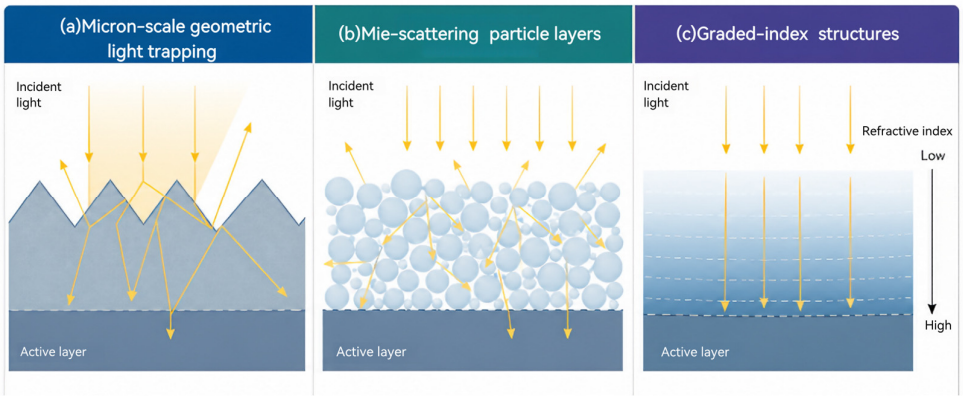


Figure 3. Optical mechanisms and conditional risks of three single-scale architectures. (**a**) Micron-scale geometric light trapping; (**b**) Mie-scattering particle layers; and (**c**) graded-index structures. Each architecture provides distinct optical benefits but also application-dependent risks, which must be evaluated using the four synergy criteria and the separate translation-readiness tier in Figure 2.

3.1. Micron-Scale Geometric Light Trapping

Micron-scale structures are the most industrially mature surface-engineering route, with feature sizes typically between 1 and 100 μm. When these features are comparable to or larger than the target wavelength, geometric optics provides a useful approximation [2,44]. Multiple internal reflections reduce light escape [46], and inclined or asymmetric structures direct transmitted light closer to the active-layer plane, extending the optical path [47]. Suitable morphology also broadens the angular response relative to a planar interface [48]. These effects can improve both antireflection and absorption, particularly in thin photovoltaic absorbers [2,22]. Hierarchical polydimethylsiloxane (PDMS) textures can also provide broadband, wide-angle light trapping [49].

Micron-scale structure design must balance size, morphology, incidence-angle range, optoelectronic performance, and process compatibility [46]. Common structures include inverted pyramids, V-grooves, microlenses, and random pyramid textures. Highly symmetric or inclined structures generally perform better at large angles, whereas smaller structures improve broadband response but increase surface recombination in active devices [2]. Wet etching, laser texturing, and additive fabrication each have boundaries in size, uniformity, and substrate compatibility. The relationship between micro/nanoscale feature size and device performance in monocrystalline silicon cells has been reviewed systematically [50]. Design evaluation cannot rely solely on reflectivity but must also consider the optoelectronic and mechanical responses of complete devices.

Periodic structures allow precise control of morphology and spacing. Inverted micropyramid arrays and vertical pyramid-thin film systems improve the broadband antireflection and photovoltaic performance of silicon devices [46]. V-groove polymethyl methacrylate (PMMA) structures are used for laser-textured low-reflectivity surfaces on silicon substrates [51]. Integrated moth-eye microlens arrays can be used for complex substrates and maintain nanostructure stability after 30 min of heating at 250 °C [52]. Pixel-level metallic blackbody microcavities achieve strong absorption in the 0.25–20 μm range, indicating that micron-scale geometries can also be used for customized spectral responses in infrared and thermal applications [53]. Single-step copper-assisted etching of inverted pyramid structures can achieve approximately 18.87% efficiency in crystalline silicon cells [54]. Inverted pyramid nanostructures are also used for broadband light trapping and efficiency improvement in polysilicon cells [55].

Random pyramid texture is suitable for low-cost, large-area manufacturing. Wet-etched random pyramids remain the standard photovoltaic process; additive-assisted potassium hydroxide (KOH) etching can improve performance while maintaining production line compatibility [2,22,56,57]. Laser-induced competitive vapor deposition expands microforest structures into aluminum films [58]. Roll-to-roll ultraviolet nanoimprinting extends hierarchical structures to flexible thin films [59]. Deterministic control of random structures remains weak. Black silicon surfaces prepared by laser micro/nanoprocessing can also form broadband, ultralow-reflectivity structures [60].

The limits of micron-scale geometries follow from the assumptions of geometric optics. As the incidence angle increases, the effective projected area and the number of internal reflections decrease, and the antireflection advantage of many systems declines rapidly. Reducing the feature size can improve broadband and angular performance, but it also increases the surface area and surface recombination [11]. In the ultraviolet and far-infrared, scattering increases when the wavelength approaches the structural dimensions, reducing the accuracy of geometric optics [46]. These limitations have motivated the use of wave-optical nanostructures.

3.2. Nanoscale Subwavelength and Resonant Structures

Nanoscale antireflective structures control light through effective-medium gradients, Mie resonance, local scattering, diffraction, and photonic-crystal effects [44,61,62]. When the lateral period is less than approximately half the wavelength, the structure can be treated as an effective medium with a graded refractive index; a fill factor that varies along the surface normal creates a smooth transition from the substrate to air and reduces reflection over a broad bandwidth [12]. Higher-order effective-medium theory corrects the errors of zero-order models at large angles and high fill factors, providing more accurate transverse-electric (TE) and transverse-magnetic (TM) responses [63]. Anisotropic nanostructures can additionally provide polarization control [64], and self-cleaning graded-index coatings may improve the transmittance of photovoltaic cover glass [65].

Mie resonance structures operate when the feature size is close to the wavelength. High-refractive-index nanoparticles, nanocolumns, and dielectric resonators can excite electric and magnetic multipoles, enhancing light absorption into the substrate or in weak absorption layers [61,66]. Unlike etched textured substrates, particle- or resonator-based structures do not require substrate etching, avoiding the recombination penalty associated with increased surface area. Photonic crystals enhance film absorption through bandgap reflection, diffraction, and extended optical path [62]. Topological interface engineering is also used to reduce backscatter and improve robustness in two-dimensional photonic crystals [67]. Mie resonance superphotonics provides a mechanistic basis for wavelength-selective light modulation [68], and subwavelength Mie resonators have been used to achieve wide-spectrum, wide-angle antireflection [69].

Typical single-nanoscale systems include etched moth-eye surfaces [12], nanoparticle or silica-microsphere layers [70], porous oxide films [13], and metasurfaces [71]. Other systems include self-assembled nanotextures [72] and photonic-crystal absorption structures [62]. Etched structures form continuous refractive-index transitions and avoid film/substrate interfaces, whereas nanoparticles and porous oxides offer greater substrate flexibility. Silica microspheres increased ultrathin-silicon absorption by about 30% in a computed result [70]. The corresponding experimental improvement in integrated reflectance was about 25%. Moth-eye structures can reduce reflection and improve transmission [73,74]. Single-layer metasurfaces can achieve broadband antireflection for silicon cells [71]. Because wavelengths, incidence conditions, and device structures differ, these results cannot be compared directly.

Nanostructures regulate spectral and angular responses through period, fill factor, height, and material [48]. High-aspect-ratio arrays and porous layers are prone to wear, scratches, contamination, and moisture absorption [13]. The large surface area of these structures also introduces recombination losses in active optoelectronic devices [11]. In contrast, moth-eye nanostructures prepared by the template method maintain broadband quasi-omnidirectional antireflection while exhibiting better structural robustness [75]. Resonant and photonic-crystal designs are usually effective only within limited spectral or angular ranges, and resonance shifts with incidence angle [61].

Practical nanoscale design requires balancing optical bandwidth, angular robustness, mechanical durability, and electrical compatibility. Graded-index subwavelength structures are suitable for wideband antireflection, resonance structures are suitable for thin film absorbers requiring optical path enhancement, and photonic crystals are suitable for spectral selectivity or in-plane coupling requirements. These functional divisions determine the applicability of nanostructures across cross-scale systems; there is no single nanomorphology suitable for all applications.

3.3. Limitations of Single-Scale Routes and Criteria for Synergy

The advantages of the three single-scale routes arise from different mechanisms. Comparisons must therefore consider bandwidth, angular response, mechanical durability, electrical compatibility, process maturity, and cost [16]. These conditions vary by application, and no single-scale solution is universally optimal. Direct comparison of the lowest reflectance values reported in different studies is also of limited value. The next section asks whether an additional scale contributes a function that cannot be achieved at a single scale and whether the gain persists at device level and under realistic process constraints.

4. Cross-Scale Composites and Synergy: Mechanisms, Evidence Criteria, and Application Mapping

4.1. Definitions and Evidence Requirements

This section evaluates cross-scale systems using the control levels defined in Section 1, with particular attention to whether single-scale controls are truly comparable. Reporting only a single performance peak may not be sufficient to support a cross-scale synergy claim. Table 2 compares the performance, process boundaries, and main limitations of three types of single-scale routes and cross-scale composite structures.

Table 2. Comparison of performance, process boundaries, and main limitations of single-scale and cross-scale antireflective structures.

Technical Route	Spectral and Angular Performance	Mechanical and Environmental Stability	Electrical Compatibility	Process Maturity and Key Limitations
Interference film	Precise design near normal incidence; performance above about 60° is limited by phase and polarization [39].	Interfacial and residual stress can reduce the laser-induced damage threshold (LIDT) [10]; adhesion, moisture uptake, and uniformity govern long-term reliability [76].	The surface area is relatively low, but interfacial recombination still depends on passivation quality [2].	Physical vapor deposition/chemical vapor deposition (PVD/CVD) is mature, low-cost, and compatible with large-area processing; refractive-index range and conformal coverage remain limiting factors [36].

Table 2. *Cont.*

Technical Route	Spectral and Angular Performance	Mechanical and Environmental Stability	Electrical Compatibility	Process Maturity and Key Limitations
Micron-scale geometry	Effective light trapping from the visible to near-infrared; antireflection performance degrades at large incidence angles [11].	The structure is integrated with the substrate, providing good mechanical and environmental stability [11].	Submicron pyramids increase the surface area by about 1.7 times, so surface passivation remains necessary [11].	Wet etching and laser texturing are relatively low-cost; electrical losses at extreme angles and submicron scales are key limitations [11].
Nanoscale subwavelength or resonant structure	Optimized subwavelength structures maintain broadband performance up to about 80°, whereas resonant structures are wavelength-selective [77].	High-aspect-ratio structures are more difficult to fabricate, and low-fill-factor graded films may degrade mechanical properties [13].	The surface area can increase substantially, raising recombination risk in active devices [11].	Large-area fabrication by conventional methods remains costly [78]; mechanical fragility, contamination, resonance bandwidth, and surface recombination require control [13,61,68].
Cross-scale composite structure	Broad-spectrum and wide-angle advantages can be combined, but performance depends on hierarchical order, scale ratio, and interface design [79].	A micron-scale skeleton can provide load bearing, and a film can provide protection, but additional interfaces and structural complexity may introduce new failure modes [80].	Partitioned passivation can reduce recombination, but it must be validated on the active interface [11].	Fabrication is complex. Wet etching, roll-to-roll nanoimprinting, and atomic layer deposition (ALD) provide examples of process compatibility, continuous replication, and conformality, respectively [11,59,81]. High-throughput ALD still lacks a common yield benchmark [82].

4.2. Synergy Mechanisms and Design

Cross-scale design distributes optical and non-optical functions across different structural levels. Micron-scale skeletons provide mechanical support, reduce the depth-to-width ratio required for nanostructures, and introduce geometric light trapping. Nanostructures provide effective refractive-index gradients, resonant coupling, or diffraction control. Continuous thin films provide passivation, protection, and admittance fine-tuning. Design evaluation should therefore use the overall response of the same device rather than combine favorable single-point results across layers.

Micron-scale light trapping and nanoscale effective-medium modulation can be combined within the same structure. For example, in an inverted-pyramid/nanopore structure, light is reflected and refracted multiple times in the micron skeleton, extending the optical path. Nanocones then form continuous refractive-index transitions that alter the local effective index or excite resonance, reducing reflection and enhancing coupling into the active layer. The average reflectance of the inverted pyramid single-scale control in this study was 13.85% at 300–800 nm, and 1.86% for the composite structure [83]. The comparison does not fully separate process variables such as radio-frequency (RF) power and does not report device-level metrics, so it only shows reduced reflection under these conditions. Submicron pyramids can combine geometric trapping and Mie scattering, reducing the air mass 1.5 global (AM1.5G) spectral-weighted reflectance by about 0.9 percentage points relative to conventional micron pyramids while maintaining low reflection from 0° to 60° [11].

Admittance matching between structured interfaces and conformal films is another path. Structured interfaces provide a basic effective refractive-index gradient, and conformal thin films adjust the local admittance. Admittance-recursive simulations suggest that this combination may improve wide-angle solar transmission, but the gain depends on structural parameters and control conditions [79]. Conformal thin films can also disperse stress and protect nanostructures; their mechanical effects must be evaluated together with optical gain under the same device conditions.

Stepwise optical management separates antireflection and light capture. The low-reflection interface first handles light injection, while the trapped-light structure in the active layer extends the optical path [47]. Thus, the same structure does not need to perform two mutually constraining tasks simultaneously. In a 100 μm thin tunnel oxide passivated contact (TOPCon) cell, the ray-tracing model compared planar structures with different textures, antireflection films, and back-surface pyramid combinations. The optimized structure was a 5 μm front-surface vertical pyramid, 60 nm/60 nm SiO_2/SiNx antireflection film, and a 1 μm back-surface vertical pyramid, simulating a short-circuit current density of 38.40 mA/cm^2 and a conversion efficiency of 21.02% [84]. These results do not fully separate the contributions of structural changes and can only serve as model clues.

Cross-scale design requires placing ray optics, wave optics, carrier transport, and mechanical reliability within the same evaluation framework. Ray tracing can model micron-scale morphology, whereas finite-difference time-domain (FDTD) or rigorous coupled-wave analysis can model nanoscale features. However, simulation alone cannot replace device verification [85]. Multi-objective design should target reflectivity, transmittance, device efficiency, surface recombination, mechanical durability, and process yield, rather than juxtaposing unrelated single-point optics. The Zernike multi-objective correction method shows that wavefront quality, reflectivity, and manufacturability can simultaneously enter the optimization process [86], but their effective ranges still require verification through independent experiments and structural variants.

Figure 2 organizes the four criteria as evidence gates. If a study compares composite structures only with single-scale results from the literature and does not control for materials, substrates, wavelengths, angles, and device processes, the conclusion is limited to the tested conditions and cannot be generalized as a universal cross-scale synergy advantage. This review uses the term "cross-scale synergy" only when all four criteria are met.

4.3. Representative Cross-Scale Systems

A common class of architectures combines micron-scale light trapping with nanoscale structures. Microstructures provide a durable skeleton and geometric light trapping, whereas nanostructures provide graded-index or resonant coupling. Periodic examples include inverted pyramid/nanopore structures [83], inverted micropyramid arrays [46], and microlens/moth-eye structures [52]; random examples include dual-scale black silicon and additive-assisted submicron pyramids. Unmasked deep reactive ion etching produced random micro/nanostructures with reflectance below 0.6% from 200 to 2500 nm and total absorption near 95%, outperforming uncombined single-scale black silicon and microstructure controls [87]. These results still require evaluation of the test conditions and device-level effects to define their applicability.

Another class combines micro/nanostructures with interference thin films. The structured interface provides broadband light management, while the film provides conformal passivation, admittance correction, or protection. SiO_2-TiO_2 broadband films deposited on structured substrates by electron-beam ion-assisted deposition had an average transmittance of 98.63% from 950 to 1064 nm and remained stable after 60 days of room-temperature

aging [88]. Graded films combined with subwavelength structures can also produce a smoother refractive-index transition and improve wide-angle transmission [79].

Wilson et al. used subwavelength features to form a graded-index transition on randomly structured antireflective surfaces [89,90]. Vaca's thesis reports that the laser-induced damage threshold (LIDT) under nanosecond pulses reached approximately ten times that of conventional antireflective thin films and approached the bulk-material threshold [89]. Because this value originates from a secondary summary and has not been independently replicated, it is treated here only as a C-level control clue. Carbon nanotube sponges and two-dimensional photonic crystals belong to adjacent optical-management routes [62,91]. Current evidence is insufficient to show that these routes satisfy the criterion of two non-overlapping scale domains or coupling between a structural scale and an independent functional layer, so they are treated only as related cases and are not classified as cross-scale synergy.

Table 3 lists studies that directly compare composite structures with single-scale controls. Panel A records the four synergy gates using V, P, N, and NR codes. Panel B records translation-readiness evidence separately. Decision rules: V requires direct evidence meeting the stated condition; P requires partial or non-matched evidence; N means no direct evidence or mechanism inference only; NR means not reported.

Table 3. (**A**) Direct-control evidence and itemized status of synergy criteria and translation readiness; (**B**) Translation-readiness evidence.

(**A**)

Study/System	Control Grade	Functional Separation	Matched Control	Device Gain	Scale Coupling/Synergy
[83] Inverted pyramid/nanopore	B	N	P	N	N/composite only
[87] Random micro/nano black silicon	B	N	P (optical)	N	N/composite only
[11] Submicron pyramids + functional film	B	N	P (device)	P	N/composite only
[48] Infrared micro/nano composite film	B	N	P (optical)	N	N/composite only

(**B**)

Study/System	Control Grade	Manufacturing	Reliability	Readiness	Interpretation
[83] Inverted pyramid/nanopore	B	NR	NR	Not ready	Optical data only
[87] Random micro/nano black silicon	B	NR	NR	Not ready	Optical/absorption data only
[11] Submicron pyramids + functional film	B	NR	NR	Not ready	Device gain, limited repeatability
[48] Infrared micro/nano composite film	B	NR	NR	Not ready	Optical metrics only

Note: The four studies in Table 3 provide mechanistic evidence, but none independently verifies functional separation.

Worked example: for [83], functional separation is N because no nanostructure-only control was reported; matched control is P because process variables and test conditions were not fully matched; device-level gain is N because only optical reflectance was reported; scale-coupling evidence is N because no additive model or scale-resolved experiment was performed. The system is therefore a cross-scale composite, not a cross-scale synergy. Translation readiness is also not established.

Table 4 lists adjacent evidence such as models, material reliability, functional extensions, manufacturing, and applications; these results are used to illustrate mechanisms or application boundaries and are not included in synergy assessment.

Table 4. Evidence of Model, Material Reliability, Functional Extension, Manufacturing and Application, etc.

Evidence Type	Representative Result	Purpose/Status	Boundary
Mechanism simulation	Comparison of transmittance between subwavelength structures and graded films [79].	Mechanistic evidence	Simulation only; no experimental control.
Device simulation	The TOPCon model achieved 38.40 mA/cm^2 and 21.02% [84].	Model input	Simulation; contributions of individual structural changes were not decoupled.
Original research and secondary summary	Wilson et al. studied nanosecond-pulse damage behavior [90]; Vaca's thesis reports that the LIDT reached approximately ten times that of conventional antireflective thin films and approached the bulk-material threshold [89].	Pending independent validation	The value comes from a secondary summary, and independent replication and reanalysis of the original data are unavailable.
Functional extension	Superhydrophobicity and wear resistance [80], antifogging [92], electromagnetic shielding [93,94], infrared stealth [95], and cross-spectral control [96].	Multifunctional extension	Different functional targets; no common antireflection control.
Material aging	SiO_2-TiO_2 films maintained an average transmittance of 98.63% at 950–1064 nm after 60 days of room-temperature aging [88].	Material stability	No matched single-scale antireflection control.
Material durability	After 120 abrasion cycles, the parallel microgroove structure maintained a contact angle of 150.2° and low reflectance [80].	Durability evidence	Material-level only; device efficiency was not reported.
Manufacturing	Roll-to-roll nanoimprinted 3D nanobowl films exhibited 98% haze and 87% transmittance [59].	Manufacturing case	Long-term device data and a common yield benchmark are lacking.
Interface and device	Textured and non-textured antireflective layers were compared in planar silicon-perovskite tandem cells [97].	Interfacial texturing evidence	This is not a comparison between a composite structure and a single-scale control.
Device application	Structural-color photovoltaic modules maintained efficiency above 21% with short-circuit current loss below 5% [98].	Multifunctional device evidence	No matched single-scale control was provided within the same study.

4.4. Manufacturing, Durability, and Measurement

The main challenge in cross-scale fabrication is to control micron-scale morphology, nanoscale features, and interface quality simultaneously. Lithography and etching typically achieve high nanoscale precision. Combining electron beam lithography with nanoimprint can control lateral offset of 50 nm features within 5%, but large-area costs remain high [99]. Displacement Talbot lithography has been used for large-area periodic structures [48]. Inductively coupled plasma etching can form high-density nanoporous structures on the surface of inverted pyramids [83].

Metal-mask reactive-ion etching has been used to prepare large-diameter random subwavelength structural samples, indicating that this route can control specific structural parameters; however, the substrates, feature diameters, and evaluation metrics differ, so a unified yield and throughput comparison is not yet possible [90].

Laser processing is suitable for curved, flexible, or chemically sensitive substrates and does not require masking. Laser micro/nanofabrication can construct multiscale structures through ablation or in situ deposition [100]. That study examined heat-affected zones and morphological uniformity. Femtosecond lasers can form hierarchical micro-nanostructures with minimal thermal damage, achieving both antireflection and superhydrophobicity [101]. Laser-induced competitive vapor deposition can create microforest structures on 50 μm aluminum films, with an average reflectance of 2.41% at 400–1200 nm [58]. Laser texturing combined with chemical etching can produce submicron pyramids compatible with crystalline silicon production lines [11] and can also form pixel-level metal blackbody microcavities with high absorption rates of 0.25–20 μm [53]. Because these studies used different substrates, structures, and objectives, their results should not be generalized into uniform limitations of laser processing.

The main indicators of the pattern replication route are continuous replication capability, defect density, and yield. Roll-to-roll ultraviolet nanoimprint can continuously fabricate flexible 3D nano-bowl films with high haze, high transmittance, and self-cleaning performance [59]. Hot embossing can replicate subwavelength antireflective gratings on polymer wafers in batch [102]. These studies demonstrate replication feasibility but do not report standardized defect-density or yield metrics.

Wet etching and atomic layer deposition represent two complementary processes. Wet etching is mature, low-cost, and compatible with existing crystalline silicon production lines; additive-assisted etching can achieve about a 1% absolute cell efficiency gain [11]. Atomic layer deposition (ALD) offers good conformality and atomic-level thickness control, forming protective or passivation layers on high aspect ratio structures [81]. High-throughput ALD is advancing toward mass manufacturing, but cost and yield still lack a unified benchmark [82]. These processes suit different substrates and structures, so engineering feasibility cannot be judged from a single performance metric.

Nanoimprinting, soft imprinting of nanowire networks, and nanogroove templates are other manufacturing cases in organic optoelectronics, transparent conductivity, and organic photovoltaics [103–105]. These routes do not share the same yield and throughput benchmarks as the inorganic silicon or oxide processes discussed above, so they are treated as extended cases rather than a unified ranking basis.

Reliability evaluation should use the same micron-, nano-, or composite-scale structures as the optical design: nanostructures may be damaged, fractured, or deformed [13], porous layers may absorb moisture [106], and active materials may also experience recombination loss due to increased surface area [11]. Ultraviolet light, high temperature, humid heat, thermal cycling, particle irradiation, and mechanical wear may all act together; structures stable in one environment may not be suitable for another. Durability data should reflect test conditions, time, and changes in optical or electrical properties, not just initial performance. For example, parallel microgroove structures formed by nanosecond laser-chemical treatment remain superhydrophobic after 120 abrasion cycles, with a contact angle of 150.2° and low reflectivity [80]. Long-term durability of sol-gel porous coatings on solar glass covers has been tracked outdoors [106].

Cross-scale studies should report measurement conditions that affect comparability: wavelength, angle, polarization, substrate, and measurement geometry. If surface recombination, mechanical durability, or process yield affects the target application, the relevant measurements or performance boundaries should be reported. Studies should also specify

the functional division of labor at each scale and report key indicators such as durability, broadband, or wide-angle absorption. For example, hierarchical-pyramid-array ultra-black films achieve both broadband wide-angle absorption and mechanical durability [107]. This information is a prerequisite for judging comparability among different studies and determines which design principles can be generalized.

4.5. Application Requirements and Route Mapping

Crystalline silicon photovoltaics are an important application scenario for antireflective films. Submicron pyramids combined with functional coatings can achieve an approximately 1 percentage point absolute efficiency gain and a 6.8% gain in outdoor daily power generation [11]. In tandem and perovskite devices, antireflective designs must also consider current matching and interface passivation between the two sub-cells [108]. Perovskite quantum dots combined with micro/nanostructures can improve efficiency through spectral conversion and interface passivation [109], and plasmonic core-shell particles can be used to enhance current collection in perovskite cells [110].

In building photovoltaics, evaluation objectives include color appearance and electrical output. Multilayer interference and surface texturing can produce structural color while maintaining >21% efficiency and keeping short-circuit current loss below 5% [98]. However, these results do not replace single-scale controls.

In fully structured tandem cells, conformal growth and interfacial texture are additional constraints. Comparing textured and non-textured antireflective layers in planar silicon-perovskite tandem cells highlights the importance of interfacial texture [97]. Periodically inverted micropyramids can achieve conformal growth and reduce reflection loss in fully structured perovskite cells [111]. These results support process and device feasibility, but single-scale control matching is still needed to determine cross-scale synergy.

Infrared imaging and optical windows require simultaneous control of mid-wave infrared (MWIR) and long-wave infrared (LWIR) reflections and stable operation over a wide angular range. When moth-eye micro/nanostructures are combined with interference effects, the average reflectance can be about 1% from 0° to 60°. The original report also states a simulation-only 35% improvement in antireflective efficiency relative to conventional films at 70–80°, but no unified basis for comparison was provided [48]. Nanostructured antireflective films can also improve the sensitivity of MWIR and LWIR detectors for remote sensing and Earth observation [112].

The evaluation targets for thermal function and infrared stealth applications differ from those of imaging windows. The aforementioned metallic blackbody microcavities can be used for thermal imaging modulation or infrared encryption [53]. Mn-based micro-nano tower structures combine solar absorption and low infrared emission, maintaining thermal stability at 300 °C [95]. These indicators reflect spectral selectivity or thermal management capabilities and cannot replace transmission and reflection indicators of the imaging window.

For high-power lasers and space systems, LIDT, radiation resistance, and long-term stability are more important than maximum bandwidth. The aforementioned LIDT clues still lack independent replication and direct control within the same batch, so this review does not include them as direct evidence [89,90]. Cover-glass thickness is used to block protons and electrons, and cerium doping suppresses darkening caused by UV irradiation [113]. Nanoarrays fabricated on cover glass can improve UV-visible light transmittance [114]. These two results correspond to different objects and cannot be used to determine that the nanoarray remains stable after irradiation. For these two types of systems, the importance of reducing interface absorption, stress concentration, and contamination sensitivity may be higher than the minimum reflectivity.

Display and augmented reality/virtual reality (AR/VR) systems also require high visible transmittance, low polarization sensitivity, low stray light, and compatibility with flexible or curved surfaces. Organic light-emitting diodes are limited by outcoupling efficiency, and nanostructures can improve light extraction; a secondary summary of random nanostructures [115] reports approximately 40% increases in current and power efficiency from the original study. Moth-eye micro/nanostructures can reduce reflection and increase transmission [74], and roll-to-roll nanoimprinting has been used to fabricate flexible 3D nanobowl films [59]. These structures also affect haze, color, and image quality, so system-level optical metrics should be reported; plasmonic enhancement can further improve the brightness and operational stability of organic light-emitting devices [116].

Multifunctional surfaces are functional extensions beyond antireflection across cross-scale structures. Hierarchical textures can simultaneously improve antireflection and superhydrophobicity [80]. Hierarchical columnar structures can simultaneously achieve antifogging and antireflective properties [92]. Conductive or dielectric shielding layers can be combined with antireflective transmission windows [93,94]. Selective absorption structures can regulate solar absorption and infrared emission [95]. These functions must be evaluated under consistent device conditions; otherwise, they remain parallel indicators rather than evidence of integration. MXene gradient frames [93], laser-etched aluminum microstructures [117], TiO_2/Au transparent hard coatings [94], and cross-scale metasurfaces [96] provide cases of electromagnetic shielding, self-cleaning, and cross-spectral regulation. Their long-term stability and large-scale manufacturing still need validation.

These application requirements, representative routes, evidence boundaries, and key bottlenecks are summarized in Table 5. The table identifies candidate routes but is not part of the evidence grading.

Table 5. Mapping application needs, representative routes, evidence boundaries, and main bottlenecks.

Application	Key Requirements	Representative Routes and Evidence Boundaries	Key Bottleneck
Crystalline-silicon photovoltaics	Broadband and wide-angle antireflection performance; low surface recombination; low cost	Geometric light trapping, graded refractive index, and surface passivation; submicron pyramids or random pyramids combined with functional films [11]; cross-scale division of labor has not been independently verified.	Trade-off between optical gain and electrical loss; large-area uniformity.
Tandem and perovskite photovoltaics	Spectral matching; current matching; interfacial passivation	Spectral matching and interfacial passivation [108]; quantum-dot spectral conversion [109]; model-suggested micro/nanostructured light management [84].	Stability under coupled optical, electrical, and environmental stresses.
Infrared imaging and optical windows	MWIR/LWIR transmission; wide-angle operation; low reflection	Graded refractive index, moth-eye structures, and selective absorption; micro/nano composite films [48]; nanostructured antireflective films improve detector sensitivity [112].	Long-term stability, contamination, and consistent optical metrics.

Table 5. *Cont.*

Application	Key Requirements	Representative Routes and Evidence Boundaries	Key Bottleneck
Space optical systems	Radiation resistance; low interfacial absorption; long-term stability	Cover glass blocks protons and electrons, and cerium doping suppresses UV-induced darkening [113]; nanoarrays on cover glass improve UV-visible transmittance [114]; stability of nanoarrays after irradiation has not been directly verified.	Radiation-resistance validation, structural defects, and performance degradation.
High-power lasers	Low reflection; high LIDT; low absorption	Random antireflective structured surfaces whose subwavelength features form a graded-index transition; LIDT values are derived from Vaca's secondary summary of Wilson's work [89,90]; independent replication is lacking.	Independent replication of LIDT data, structural defects, and damage initiation.
Displays and AR/VR	Low visible reflection; low polarization sensitivity; flexible substrates	Outcoupling, graded refractive index, and conformal replication; moth-eye films, metasurfaces, and cross-scale light extraction [74,115,116]; system-level metric definitions remain nonuniform.	Haze, color shift, stray light, and scalable replication; joint validation in actual devices is required.

These routes indicate that no single cross-scale structure applies to all applications. The priority route depends on the relative importance of bandwidth, angular tolerance, mechanical durability, electrical loss, and manufacturing scale. Application-centered evaluation is more practical than a unified ranking based on laboratory reflectivity.

5. Conclusions

5.1. Conclusions Supported by Current Evidence

The reviewed literature supports a limited set of claims. Interference thin films remain the most mature antireflective technology; microstructures provide durable light trapping, and nanostructures extend design space through effective-medium theory, resonance, and diffraction. Among the studies included in this review, the four direct-control studies listed in Table 3 contain same-study single-scale comparisons, but none provides direct scale-coupling evidence, and each lacks at least device-level replication, environmental reliability, or manufacturing constraints. No included study meets all four synergy criteria. The laser-induced damage threshold (LIDT) clue remains a secondary summary [89,90], and the tunnel oxide passivated contact (TOPCon) values are simulation-only [84]. The evidence supports specific structures under specific conditions; it does not establish a universal advantage of cross-scale synergy.

5.2. Remaining Evidence Gaps

The conclusions of this review are limited by the literature coverage and classification framework, and studies outside the selected scope may have been omitted. A/B/C denotes control level only and does not replace reanalysis of the original data. Four evidence gaps define the boundaries of the present conclusions.

Multiscale models still struggle to simultaneously cover optical response, carrier transport, and mechanical failure, as these processes operate at different scales and time constants. Existing methods provide approximations but have limited accuracy for disor-

dered structures, dynamic interfaces, and coupled electrical effects [72,85]. If the model only predicts reflectance but cannot predict recombination, stress, or process sensitivity, it is difficult to guide device design.

Long-term reliability still lacks comparable data: nano and porous surfaces may degrade due to wear, contamination, moisture absorption, UV exposure, or thermal cycling. Protective layers can improve durability but alter optical admittance and introduce new interfaces [79,81]. Reliability studies require simultaneous reporting of morphology, interface chemistry, and changes in optical or electrical properties.

Manufacturing scale-up remains limited by yield and cost. Lithography offers high precision but is expensive over large areas. Wet etching, roll-to-roll nanoimprinting, and atomic layer deposition each require trade-offs among precision, throughput, and compatibility [11,59,81]. Laboratory research can only support production conversion by providing defect statistics, process windows, and yields.

Performance coupling makes single-indicator optimization inadequate for predicting device outcomes: antireflective layers affect surface passivation [11], mechanical durability [80], spectral selectivity [95], and self-cleaning or electromagnetic shielding [93,94]. Design objectives should therefore specify optical, electrical, mechanical, environmental, and manufacturing constraints simultaneously.

5.3. Priorities for Future Research

Future research should first strengthen comparative design: single-scale and cross-scale structures should be compared within the same batch or on the same device and under the same test conditions, and repeatable device-level metrics should be reported to determine the source of gain.

Second, optical, electrical, mechanical, and reliability metrics should be incorporated into the same optimization or inversion process and verified through independent experiments; the test scope should cover extreme angles, resonance mismatches, damp heat, irradiation, and mechanical wear, and if synergistic benefits occur, their vanishing boundaries should also be provided [13,85,86,106].

Manufacturing research should also report defect density, yield, and cost per unit area, and establish comparable indicators among roll-to-roll, wet etching, and atomic layer deposition routes [11,59,81,99]. Multifunctional integration requires joint evaluation indicators [80,107]. Composite-band antireflection surfaces based on guided-mode resonance beyond the subwavelength condition are another direction for further exploration [118].

Overall, cross-scale surface engineering is an evidence-constrained design strategy rather than an inherently superior replacement for single-scale schemes. In this review, cross-scale synergy is claimed only when functional separation, a matched control, repeatable device-level gain, and scale-coupling evidence are all established. Translation readiness is assessed separately through manufacturing and reliability evidence. The reviewed studies support composite formation and selected performance gains, but not a completed synergy claim.

Author Contributions: Conceptualization, S.Z.; methodology, data curation, and writing—original draft preparation, S.Z.; formal analysis, E.Z.; writing—review and editing, S.L.; supervision, S.L. All authors have read and agreed to the published version of the manuscript.

Funding: "3510" Medical Innovation Leadership Program, Fundamental Research Funds for the Central Universities, Sun Yat-sen University, grant number 20263510YXQN015.

Institutional Review Board Statement: Not applicable.

Data Availability Statement: No new data were created or analyzed in this study. Data sharing is not applicable to this article.

Conflicts of Interest: The authors declare no conflicts of interest.

References

1. MacLeod, H.A. *Thin-Film Optical Filters*; CRC Press: Boca Raton, FL, USA, 2010. [CrossRef]
2. Shanmugam, N.; Pugazhendhi, R.; Madurai Elavarasan, R.; Kasiviswanathan, P.; Das, N. Anti-Reflective Coating Materials: A Holistic Review from PV Perspective. *Energies* **2020**, *13*, 2631. [CrossRef]
3. Hang, L.; You, Y.; Yang, Y.; Song, S.; Zhang, Y.; Song, J.; Cheng, J.; Zhu, Y.; Liang, H.; Xu, J.; et al. Graded-index anti-reflection coatings with high-power laser-induced damage resistance and high transmittance based on a SiOxNy layer deposited by PECVD. *Opt. Laser Technol.* **2026**, *197*, 114859. [CrossRef]
4. Ding, Y.; Wang, C.; Jia, X.; Liu, L.; Gao, Z.; Jiang, X.; Wang, S.; Yan, D.; Lin, N.; Li, Z.; et al. Laser-optical-field-modulation fabricating large-aperture dual-band antireflection windows for MWIR and LWIR imaging. *Int. J. Extrem. Manuf.* **2025**, *8*, 025004. [CrossRef]
5. Bashir Khan, S.; Wu, H.; Pan, C.; Zhang, Z. A Mini Review: Antireflective Coatings Processing Techniques, Applications and Future Perspective. *Res. Rev. J. Mater. Sci.* **2017**, *5*, 1–19. [CrossRef]
6. Ji, C.; Liu, W.; Bao, Y.; Chen, X.; Yang, G.; Wei, B.; Yang, F.; Wang, X. Recent Applications of Antireflection Coatings in Solar Cells. *Photonics* **2022**, *9*, 906. [CrossRef]
7. Song, J.-K.; Wu, S.-T. Optical Materials and Applications for AR and VR Display Systems. *ACS Appl. Opt. Mater.* **2024**, *2*, 1245–1246. [CrossRef]
8. Butt, M.A.; Tyszkiewicz, C.; Karasiński, P.; Zięba, M.; Kaźmierczak, A.; Zdończyk, M.; Duda, Ł.; Guzik, M.; Olszewski, J.; Martynkien, T.; et al. Optical Thin Films Fabrication Techniques—Towards a Low-Cost Solution for the Integrated Photonic Platform: A Review of the Current Status. *Materials* **2022**, *15*, 4591. [CrossRef]
9. Horodynski, M.; Kühmayer, M.; Ferise, C.; Rotter, S.; Davy, M. Anti-reflection structure for perfect transmission through complex media. *Nature* **2022**, *607*, 281–286. [CrossRef]
10. Long, G.; Zhang, Y.; Zhou, H.; Fan, X.; Zhang, X.; Yang, Z.; Li, E. Ultra-low stress and high laser damage threshold optical coatings for large-aperture component. *Opt. Laser Technol.* **2025**, *184*, 112297. [CrossRef]
11. Zhong, S.; Qian, C.; Yu, F.; Wu, Z.; Huang, Z.; Yin, H.; Zhang, J.; Xu, H.; Xu, R.; Shen, W. Surface texturing for advanced light management in crystalline silicon solar cells: From submicron pyramid fabrication to outdoor validation. *Renew. Energy* **2026**, *256*, 124546. [CrossRef]
12. Yang, H.; Pu, J.; Lu, L. Anti-reflective engineering via moth-eye-inspired nanostructures: Fundamental principles, fabrications, and applications. *Renew. Sustain. Energy Rev.* **2026**, *231*, 116785. [CrossRef]
13. Han, Z.; Jiao, Z.; Niu, S.; Ren, L. Ascendant bioinspired antireflective materials: Opportunities and challenges coexist. *Prog. Mater. Sci.* **2019**, *103*, 1–68. [CrossRef]
14. Huang, Y.-F.; Chattopadhyay, S.; Jen, Y.-J.; Peng, C.-Y.; Liu, T.-A.; Hsu, Y.-K.; Pan, C.-L.; Lo, H.-C.; Hsu, C.-H.; Chang, Y.-H.; et al. Improved broadband and quasi-omnidirectional anti-reflection properties with biomimetic silicon nanostructures. *Nat. Nanotechnol.* **2007**, *2*, 770–774. [CrossRef]
15. Wang, W.; Qi, L. Light Management with Patterned Micro- and Nanostructure Arrays for Photocatalysis, Photovoltaics, and Optoelectronic and Optical Devices. *Adv. Funct. Mater.* **2019**, *29*, 1807275. [CrossRef]
16. Raut, H.K.; Ganesh, V.A.; Nair, A.S.; Ramakrishna, S. Anti-reflective coatings: A critical, in-depth review. *Energy Environ. Sci.* **2011**, *4*, 3779. [CrossRef]
17. Li, C.; Liang, L.; Zhang, B.; Yang, Y.; Ji, G. Magneto-Dielectric Synergy and Multiscale Hierarchical Structure Design Enable Flexible Multipurpose Microwave Absorption and Infrared Stealth Compatibility. *Nano-Micro Lett.* **2024**, *17*, 40. [CrossRef]
18. Nepal, D.; Kang, S.; Adstedt, K.M.; Kanhaiya, K.; Bockstaller, M.R.; Brinson, L.C.; Buehler, M.J.; Coveney, P.V.; Dayal, K.; El-Awady, J.A.; et al. Hierarchically structured bioinspired nanocomposites. *Nat. Mater.* **2022**, *22*, 18–35. [CrossRef]
19. Dingreville, R.; Karnesky, R.A.; Puel, G.; Schmitt, J.-H. Review of the synergies between computational modeling and experimental characterization of materials across length scales. *J. Mater. Sci.* **2015**, *51*, 1178–1203. [CrossRef]
20. van der Giessen, E.; Schultz, P.A.; Bertin, N.; Bulatov, V.V.; Cai, W.; Csányi, G.; Foiles, S.M.; Geers, M.G.D.; González, C.; Hütter, M.; et al. Roadmap on multiscale materials modeling. *Model. Simul. Mater. Sci. Eng.* **2020**, *28*, 043001. [CrossRef]
21. Chen, Y.; Montes McNeil, A.; Park, T.; Wilson, B.A.; Iyer, V.; Bezick, M.; Choi, J.-I.; Ojha, R.; Mahendran, P.; Singh, D.K.; et al. Machine-learning-assisted photonic device development: A multiscale approach from theory to characterization. *Nanophotonics* **2025**, *14*, 3761–3793. [CrossRef]
22. Ali, S.M.; Karasu, Y.E. A Review of Anti-Reflective Coating Technologies for PV Systems: Materials, Designs, and Performance Enhancement. In Proceedings of the 6th International Conference on Frontiers in Academic Research, Konya, Turkey, 16–17 December 2025; Conference Proceedings; pp. 279–289. Available online: https://drive.google.com/file/d/1u0-1Xd-9gyPqzKvFu2jGKkYHsXEiBhu3/view (accessed on 22 October 2026).

23. Grant, M.J.; Booth, A. A typology of reviews: An analysis of 14 review types and associated methodologies. *Health Inf. Libr. J.* **2009**, *26*, 91–108. [CrossRef]
24. Basu, B.; Ghosh, S. Assessment of Technology and Manufacturing Readiness Levels. In *Biomaterials for Musculoskeletal Regeneration*; Indian Institute of Metals Series; Springer: Singapore, 2016; pp. 235–246. [CrossRef]
25. Rybicka, J.; Tiwari, A.; Leeke, G.A. Technology readiness level assessment of composites recycling technologies. *J. Clean. Prod.* **2016**, *112*, 1001–1012. [CrossRef]
26. Jones, M.; Webb, P.; Summers, M.; Baguley, P. A manufacturing technology readiness impact assessment transitional framework. In Proceedings of the 2012 IEEE Aerospace Conference, Big Sky, MT, USA, 3–10 March 2012; pp. 1–9. [CrossRef]
27. Azzam, R.M.A. Polarization, thin-film optics, ellipsometry, and polarimetry: Retrospective. *J. Vac. Sci. Technol. B* **2019**, *37*, 060802. [CrossRef]
28. Kipnis, N. Fresnel and the principle of interference. In *History of the Principle of Interference of Light*; Springer: Berlin/Heidelberg, Germany, 1991; pp. 165–198. [CrossRef]
29. Luce, A.; Mahdavi, A.; Marquardt, F.; Wankerl, H. TMM-Fast, a transfer matrix computation package for multilayer thin-film optimization: Tutorial. *J. Opt. Soc. Am. A* **2022**, *39*, 1007. [CrossRef]
30. Ma, T.; Ma, M.; Guo, L.J. Optical multilayer thin film structure inverse design: From optimization to deep learning. *iScience* **2025**, *28*, 112222. [CrossRef]
31. Oktay, S.; Duru, İ.; Bakır, H.; Tabaru, T.E. Deep learning and machine learning based highly accurate reflection prediction model for multi layers anti-reflection coatings. *Opt. Quantum Electron.* **2025**, *57*, 101. [CrossRef]
32. Marchand, E.W. *Gradient Index Optics*; Academic Press: Cambridge, MA, USA, 1978. Available online: https://shop.elsevier.com/books/gradient-index-optics/marchand/978-0-12-470750-4 (accessed on 22 October 2026).
33. Anzengruber, S.W.; Klann, E.; Ramlau, R.; Tonova, D. Numerical methods for the design of gradient-index optical coatings. *Appl. Opt.* **2012**, *51*, 8277. [CrossRef]
34. Yang, Y.-T.; Cai, Q.-Y.; Li, F.-X.; Hu, E.-T.; Liu, B.-J.; Luo, H.-H.; Zhang, R.-J.; Li, J.; Zheng, Y.-X.; Duan, W.-B. Fabrication of antireflection coatings from visible to mid-wave infrared via quantitative control of the refractive index. *Opt. Express* **2026**, *34*, 3676. [CrossRef]
35. Chen, D. Anti-reflection (AR) coatings made by sol–gel processes: A review. *Sol. Energy Mater. Sol. Cells* **2001**, *68*, 313–336. [CrossRef]
36. Tusher, M.M.H.; Imam, A.; Shuvo, M.S.I. Future and Challenges of Coating Materials. In *Coating Materials*; Materials Horizons: From Nature to Nanomaterials; Springer: Singapore, 2023; pp. 229–251. [CrossRef]
37. Bousbih, R.; Dimassi, W.; Haddadi, I.; Ben Slema, S.; Rava, P.; Ezzaouia, H. Silicon Lifetime Enhancement by SiNx:H Anti-Reflective Coating Deposited by PECVD Using SiH4 and N2 Reactive Gas. *Sol. Energy* **2012**, *86*, 1300–1305. [CrossRef]
38. You, D.; Jiang, Y.; Cao, Y.; Guo, W.; Tan, M. Broadband antireflective coatings in the optical communication band deposited by ion-assisted reactive magnetron sputtering. *Infrared Phys. Technol.* **2023**, *131*, 104664. [CrossRef]
39. Willey, R.R. *Practical Design and Production of Optical Thin Films*; CRC Press: Boca Raton, FL, USA, 2002. [CrossRef]
40. Peng, Q.; Zaheer, S.M.; Li, J.; Rehman, J.; Shafiee, S.A.; Masood, M.K.; Alsaiari, N.S. Enhancing optical absorption and efficiency of perovskite solar cells using embedded ag nanoparticles array and ITO moth-eye anti-reflective layers. *Opt. Quantum Electron.* **2026**, *58*, 69. [CrossRef]
41. He, C.; Fu, X.; Zhang, J.; Li, S. Study and Fabrication of Visible and IR Dual-Band Broadband Antireflection Coating. *Acta Opt. Sin.* **2009**, *29*, 2929–2933. [CrossRef]
42. Fang, Z.; Chen, Q.; Yuan, J. Bi-layered closed-pore structure anti-reflective coatings with ZnO quantum dots for further improving the solar cell efficiency. *Sol. Energy Mater. Sol. Cells* **2026**, *294*, 113936. [CrossRef]
43. Kaiser, N.; Pulker, H.K. *Optical Interference Coatings*; Springer Series in Optical Sciences; Springer: Berlin/Heidelberg, Germany, 2003. [CrossRef]
44. Chattopadhyay, S.; Huang, Y.-F.; Jen, Y.-J.; Ganguly, A.; Chen, K.-H.; Chen, L.-C. Anti-reflecting and photonic nanostructures. *Mater. Sci. Eng. R Rep.* **2010**, *69*, 1–35. [CrossRef]
45. Liu, C.; Hou, X.; Zhu, Z.; Li, M. Bioinspired micro-nano photonic materials. *Chem. Soc. Rev.* **2025**, *54*, 8434–8468. [CrossRef]
46. Srivastava, A.; Sharma, D.; Laxmi, S.; Tawale, J.S.; Pathi, P.; Srivastava, S.K. Excellent omnidirectional light trapping properties of inverted micro-pyramid structured silicon by copper catalyzed chemical etching. *Opt. Mater.* **2022**, *131*, 112677. [CrossRef]
47. Ryckaert, S.R. Light-Trapping in Ultra-Thin Solar Cells. Research Report, Centre de Nanosciences et Nanotechnologies 2025. Master's Thesis, Politecnico di Torino, Torino, Italy, 2025. Available online: https://webthesis.biblio.polito.it/37890/1/tesi.pdf (accessed on 22 October 2026).
48. Yang, J.; Yang, J.; Fu, Y.; Wu, J.; Ouyang, M.; Dong, L.; Kou, S. Design and manufacturing of mid-infrared ultra-wide-angle antireflective composite micro-nano structure film. *Opt. Mater.* **2024**, *149*, 115137. [CrossRef]
49. Lee, H.; Chae, S.; Yi, A.; Devaraj, V.; Oh, J.-W.; Cho, I.H.; Kim, H.J. Optimization of hierarchical textured PDMS film with wide-angle broadband anti-reflection for light trapping in solar cells. *Chem. Eng. J.* **2024**, *502*, 157155. [CrossRef]

50. Liu, H.; Du, Y.; Yin, X.; Bai, M.; Liu, W. Micro/Nanostructures for Light Trapping in Monocrystalline Silicon Solar Cells. *J. Nanomater.* **2022**, *2022*, 8139174. [CrossRef]
51. Liang, L.; Liu, W.; Cao, Y.; Zhu, D.; Zhang, J.; Yu, Y. Light trapping PMMA planar ridged waveguide on a laser textured silicon substrate for ultra-low reflectivity. *Opt. Laser Technol.* **2022**, *154*, 108341. [CrossRef]
52. Nakamura, M.; Mano, I.; Taniguchi, J. Fabrication of micro-lens array with antireflection structure. *Microelectron. Eng.* **2019**, *211*, 29–36. [CrossRef]
53. Ng, C.-K.; Chen, T.; Ju, B.-F.; Chen, Y.-L.; Ma, Y. Pixel-level metal blackbody microcavities via hierarchical laser writing. *Sci. Adv.* **2025**, *11*, eadu0608. [CrossRef]
54. Yang, L.; Liu, Y.; Wang, Y.; Chen, W.; Chen, Q.; Wu, J.; Kuznetsov, A.; Du, X. 18.87–efficient inverted pyramid structured silicon solar cell by one-step Cu-assisted texturization technique. *Sol. Energy Mater. Sol. Cells* **2017**, *166*, 121–126. [CrossRef]
55. Jiang, Y.; Shen, H.; Pu, T.; Zheng, C.; Tang, Q.; Gao, K.; Wu, J.; Rui, C.; Li, Y.; Liu, Y. High efficiency multi-crystalline silicon solar cell with inverted pyramid nanostructure. *Sol. Energy* **2017**, *142*, 91–96. [CrossRef]
56. Alasfour, A.; Yu, Z.J.; Weigand, W.; Quispe, D.; Holman, Z.C. Sub-micrometer random-pyramid texturing of silicon solar wafers with excellent surface passivation and low reflectance. *Sol. Energy Mater. Sol. Cells* **2020**, *218*, 110761. [CrossRef]
57. Abdel Naser, S.; Diab, A.A.Z.; Al Dawsari, S.; Ismeil, M.A.; Zahran, M. Monocrystalline silicon solar cell efficiency dependence on potassium silicate additive in texturing process with a study on the effect of the active material. *PLoS ONE* **2026**, *21*, e0348411. [CrossRef]
58. Chen, Q.; Duan, J.; Xiong, W.; Deng, L. High-performance anti-reflection micro-forests on aluminium alloy fabricated by laser induced competitive vapor deposition. *Opt. Express* **2023**, *31*, 12802. [CrossRef]
59. Zhang, J.; Li, C.; Li, Z.; Ren, Z.; Li, X.; Tang, Y.; Liu, G.; Zhu, X.; Qiu, Y.; Tian, H.; et al. R2R fabrication of multiply indented, hybrid 3D-nanobowls with ultra-high haze for efficiently light trapping. *Nano Res.* **2026**, *19*, 94908395. [CrossRef]
60. Yang, J.; Luo, F.; Kao, T.S.; Li, X.; Ho, G.W.; Teng, J.; Luo, X.; Hong, M. Design and fabrication of broadband ultralow reflectivity black Si surfaces by laser micro/nanoprocessing. *Light Sci. Appl.* **2014**, *3*, e185. [CrossRef]
61. Dorodnyy, A.; Smajic, J.; Leuthold, J. Mie Scattering for Photonic Devices. *Laser Photonics Rev.* **2023**, *17*, 2300055. [CrossRef]
62. Bouras, M.; Hadjab, M.; Chahmi, M.; Khennouf, S.; Rabehi, A.; Agajie, T.F.; Alanazi, A.K. Enhanced light trapping in thin-films perovskite solar cells by photonic crystal structures. *AIP Adv.* **2026**, *16*, 015116. [CrossRef]
63. Lalanne, P.; Hugonin, J.-P. High-order effective-medium theory of subwavelength gratings in classical mounting: Application to volume holograms. *J. Opt. Soc. Am. A* **1998**, *15*, 1843. [CrossRef]
64. Li, Z.; Liu, W.; Zhang, Y.; Cheng, H.; Zhang, S.; Chen, S. Optical polarization manipulations with anisotropic nanostructures. *PhotoniX* **2024**, *5*, 30. [CrossRef]
65. He, E.; Cheng, S.; Sutar, R.S.; Latthe, S.; Xing, R.; Liu, S. Self-cleaning and antireflection dual-functional gradient-index coatings for enhanced light harvesting in photovoltaic panels. *Prog. Org. Coat.* **2026**, *210*, 109674. [CrossRef]
66. Ha, D.; Gong, C.; Leite, M.S.; Munday, J.N. Demonstration of Resonance Coupling in Scalable Dielectric Microresonator Coatings for Photovoltaics. *ACS Appl. Mater. Interfaces* **2016**, *8*, 24536–24542. [CrossRef]
67. Novák, O.; Herranz, G.; Veis, M. Methodology for Topological Interface Engineering in 2D Photonic Crystals. *Adv. Photonics Res.* **2025**, *7*, e202500135. [CrossRef]
68. Babicheva, V.E.; Evlyukhin, A.B. Mie-resonant metaphotonics. *Adv. Opt. Photonics* **2024**, *16*, 539. [CrossRef]
69. Spinelli, P.; Verschuuren, M.A.; Polman, A. Broadband omnidirectional antireflection coating based on subwavelength surface Mie resonators. *Nat. Commun.* **2012**, *3*, 692. [CrossRef]
70. Banerjee, P.; Roy, A.B.; Nandi, A.; Das, S.; Kundu, A.; Mukherjee, S.; Saha, H.; Hossain, S.M. Light-trapping scheme using silica spheres on ultrathin c-silicon absorber: Transition from antireflection coating to whispering gallery resonator. *Appl. Phys. A* **2022**, *128*, 481. [CrossRef]
71. Ovcharenko, A.; Polevoy, S.; Yermakov, O. Forward and inverse design of single-layer metasurface-based broadband antireflective coating for silicon solar cells. *Adv. Photonics Nexus* **2025**, *4*, 036009. [CrossRef]
72. Rahman, A.; Ashraf, A.; Xin, H.; Tong, X.; Sutter, P.; Eisaman, M.D.; Black, C.T. Sub-50-nm self-assembled nanotextures for enhanced broadband antireflection in silicon solar cells. *Nat. Commun.* **2015**, *6*, 5963. [CrossRef]
73. Chan, L.W.; Morse, D.E.; Gordon, M.J. Moth eye-inspired anti-reflective surfaces for improved IR optical systems & visible LEDs fabricated with colloidal lithography and etching. *Bioinspir. Biomim.* **2018**, *13*, 041001. [CrossRef]
74. Zhao, L.; Guo, Y.; Kang, T.; Jiang, Y.; Zhang, H.; Zhang, H. Preparation and Study of Moth-Eye-Like Micro-Nano Structure Optical Anti-Reflection Coating. *Polym. Sci. Ser. B* **2024**, *66*, 182–192. [CrossRef]
75. Jin, B.; He, J. Self-Templated Fabrication of Robust Moth-Eye-Like Nanostructures with Broadband and Quasi-Omnidirectional Antireflection Properties. *ACS Photonics* **2016**, *4*, 188–196. [CrossRef]
76. Olasoji, A.J.; Im, S.H. Challenges and Research Directions in Optical Coatings for Future Display Technologies: Focus on Adhesion, Durability, and Optical Uniformity. In *Functional Coating Layers for Surface Engineering of Electronic Displays*; SpringerBriefs in Applied Sciences and Technology; Springer: Cham, Switzerland, 2026; pp. 103–120. [CrossRef]

77. Chae, S.; Lee, C.; Kim, Y.; Park, Y.; Kim, Y.; Lee, S.; Kim, U.J. Near-infrared antireflection coating operated with broad incident angles. *J. Korean Phys. Soc.* **2024**, *86*, 68–72. [CrossRef]
78. Modaresialam-Bochet, M. Fabrication of Dielectric Nanostructures by Nano Imprint Lithography and Sol-Gel Chemistry for Optical Applications. Ph.D. Thesis, Aix-Marseille Université, Marseille, France, 2022. [CrossRef]
79. Zhu, Z.; Bu, Y.; Wang, X. Modeling and admittance recursive simulation of anti-reflective coatings for photothermal conversion: Synergy between subwavelength structures and gradient refractive index layers. *Phys. Chem. Chem. Phys.* **2024**, *26*, 19755–19774. [CrossRef]
80. Wang, H.; Zhuang, J.; Yu, J.; Qi, H.; Ma, Y.; Wang, H.; Guo, Z. Fabrication of Anti-Reflective Surface with Superhydrophobicity/High Oleophobicity and Enhanced Mechanical Durability via Nanosecond Laser Surface Texturing. *Materials* **2020**, *13*, 5691. [CrossRef]
81. Zhang, J.; Coll, M.; Puig, T.; Pellicer, E.; Sort, J. Conformal oxide nanocoatings on electrodeposited 3D porous Ni films by atomic layer deposition. *J. Mater. Chem. C* **2016**, *4*, 8655–8662. [CrossRef]
82. Muñoz-Rojas, D.; Maindron, T.; Estève, A.; Piallat, F.; Kools, J.C.S.; Decams, J.-M. Speeding up the unique assets of atomic layer deposition. *Mater. Today Chem.* **2019**, *12*, 96–120. [CrossRef]
83. Fan, Z.; Xu, L.; Zhou, B.; Chen, T. Fabrication of Anti-Reflective Composite Structures on Inverted Pyramids Using Inductively Coupled Plasma Etching. *Micromachines* **2025**, *16*, 503. [CrossRef]
84. Fuad, M.F.B.M.; Rashid, M.M.M.; Pakhuruddin, M.Z. Ray Tracing of Light Trapping Strategies in Thin Silicon Solar Cells based on Tunnel Oxide Passivated Contact (TOPCon). *Silicon* **2026**, *18*, 1215–1230. [CrossRef]
85. Riganti, R.; Zhu, Y.; Cai, W.; Torquato, S.; Dal Negro, L. Multiscale Physics-Informed Neural Networks for the Inverse Design of Hyperuniform Optical Materials. *Adv. Opt. Mater.* **2025**, *13*, 2403304. [CrossRef]
86. Hong, L.; Song, H.; Zhang, L.; Wang, X. Zernike Correction and Multi-Objective Optimization of Multi-Layer Dual-Scale Nano-Coupled Anti-Reflective Coatings. *Modelling* **2026**, *7*, 29. [CrossRef]
87. Zhang, X.; Di, Q.; Zhu, F.; Sun, G.; Zhang, H. Wideband anti-reflective micro/nano dual-scale structures: Fabrication and optical properties. *Micro Nano Lett.* **2011**, *6*, 947–950. [CrossRef]
88. Muthusamy, O.; Joya, Y.; Day, R.; Nyamayaro, C.; Assinder, B.; Khan, S.; Jevon, M.; Wang, Z. Electron beam ion-assisted deposition of SiO_2–TiO_2 broadband antireflection coatings: Substrate temperature effect on optical properties. *Surf. Interfaces* **2026**, *90*, 109259. [CrossRef]
89. Vaca, B. Anti-Reflective Structured Surfaces on Optical Windows Through Tunable Metallic Etch Masking. Master's Thesis, University of North Carolina at Charlotte, Charlotte, NC, USA, 2024. Available online: https://ninercommons.charlotte.edu/record/2973/?ln=en (accessed on 22 October 2026).
90. Wilson, C.R.; Hutchens, T.C.; Sapkota, G.; Case, J.R.; Potter, M.G.; Busse, L.E.; Frantz, J.A.; Shaw, L.B.; Sanghera, J.S.; Poutous, M.K.; et al. Laser damage of silica optical windows with random antireflective structured surfaces. *Opt. Eng.* **2018**, *57*, 121906. [CrossRef]
91. Zhan, H.; Shi, Q.Q.; Wu, G.; Wang, J.N. Construction of Carbon Nanotube Sponges to Have High Optical Antireflection and Mechanical Stability. *ACS Appl. Mater. Interfaces* **2020**, *12*, 16762–16771. [CrossRef]
92. Li, W.; Chen, Y.; Jiao, Z. Efficient Anti-Fog and Anti-Reflection Functions of the Bio-Inspired, Hierarchically-Architectured Surfaces of Multiscale Columnar Structures. *Nanomaterials* **2023**, *13*, 1570. [CrossRef]
93. Chen, L.; Mai, T.; Guo, Z.-H.; Liu, Q.; Lang, J.-Q.; Ma, M.-G. 3D-printed MXene-based gradient framework for enhanced anti-reflection performance and excellent electromagnetic interference shielding with multi-scene adaptability. *Chem. Eng. J.* **2025**, *513*, 162871. [CrossRef]
94. Gao, G.; Huang, Y.; Zeng, S.; Li, K.; Zhang, Y.; Zhu, J. Transparent and hard TiO2/Au electromagnetic shielding antireflection coatings on aircraft canopy PMMA organic glass. *Appl. Surf. Sci.* **2024**, *658*, 159830. [CrossRef]
95. Zhang, Y.; Feng, G.; Tan, S.; Zhou, M.; Gu, W.; Guan, X.; Xu, T.; Miao, S.; Ji, G. Mn0.6Ni1.4Co2Oy micro-nano tower structure with tunable spectral selectivity interface for infrared stealth and solar selective coating application. *Prog. Org. Coat.* **2024**, *187*, 108172. [CrossRef]
96. Lin, H.; Shen, F.; Zhang, Z.; Luo, J.; Huang, C.; Pu, M.; Wang, Y.; Shi, J.; Ma, X.; Luo, X. Trans-scale hierarchical metasurfaces for multispectral compatible regulation of lasers, infrared light, and microwaves. *Nanophotonics* **2025**, *14*, 2939–2952. [CrossRef]
97. Spence, M.; Hammond, R.; Pockett, A.; Wei, Z.; Johnson, A.; Watson, T.; Carnie, M.J. A Comparison of Different Textured and Non-Textured Anti-Reflective Coatings for Planar Monolithic Silicon-Perovskite Tandem Solar Cells. *ACS Appl. Energy Mater.* **2022**, *5*, 5974–5982. [CrossRef]
98. Xu, Z.; Matsui, T.; Matsubara, K.; Sai, H. Effect of multilayer structure and surface texturing on optical and electric properties of structural colored photovoltaic modules for BIPV applications. *Appl. Energy* **2024**, *367*, 123347. [CrossRef]
99. Xu, S.; Ge, S.; Sun, Z.; Li, J.; Shi, R.; Shen, L.; Zhang, J.; Xi, Y. The Research on Multi-Process Collaborative Manufacturing and Characterization Methods of Micro–Nano-Composite Layered Structures. *Nanomaterials* **2025**, *15*, 1716. [CrossRef]

100. Chen, T.; Wang, W.; Pan, A.; Hu, L.; Mei, X. Characterization of anti-reflection structures fabricated via laser micro/nano-processing. *Opt. Mater.* **2022**, *131*, 112686. [CrossRef]
101. Duan, J.; Long, G.; Xu, X.; Liu, W.; Li, C.; Chen, L.; Zhang, J.; Xiao, J. Hierarchical Micro/Nanostructures with Anti-Reflection and Superhydrophobicity on the Silicon Surface Fabricated by Femtosecond Laser. *Micromachines* **2024**, *15*, 1304. [CrossRef]
102. Dávid, C.; Häberling, P.; Schnieper, M.; Söchtig, J.; Zschokke, C. Nano-structured anti-reflective surfaces replicated by hot embossing. *Microelectron. Eng.* **2002**, *61–62*, 435–440. [CrossRef]
103. Song, N.; Guo, X.; Zhao, H.; Li, B.; Liang, N.; Zhai, T. Nanoimprint Lithography Enabling High-Performance Organic Optoelectronics: Advances and Perspectives. *Nano-Micro Lett.* **2026**, *18*, 236. [CrossRef]
104. van de Groep, J.; Gupta, D.; Verschuuren, M.A.; Wienk, M.M.; Janssen, R.A.J.; Polman, A. Large-area soft-imprinted nanowire networks as light trapping transparent conductors. *Sci. Rep.* **2015**, *5*, 11414. [CrossRef]
105. Chowdhury, D.; Mohamed, S.A.; Manzato, G.; Siri, B.; Chittofrati, R.; Giordano, M.C.; Hussein, M.; Hameed, M.F.O.; Obayya, S.S.A.; Stadler, P.; et al. Broadband Photon Harvesting in Organic Photovoltaic Devices Induced by Large-Area Nanogrooved Templates. *ACS Appl. Nano Mater.* **2023**, *6*, 6230–6240. [CrossRef]
106. San Vicente, G.; Bayón, R.; Germán, N.; Morales, Á. Long-term durability of sol–gel porous coatings for solar glass covers. *Thin Solid Films* **2009**, *517*, 3157–3160. [CrossRef]
107. Li, H.; Xu, J.; Gao, Y.; Piao, M.; Wang, X.; Li, C.; Shi, H. Hierarchical Pyramid-Array-Based Robust Superblack Sheets With Excellent Mechanical Durability for Broadband and Wide-Angle Absorption. *Adv. Opt. Mater.* **2026**, *14*, e03035. [CrossRef]
108. Ying, Z.; Yang, X.; Wang, X.; Ye, J. Towards the 10-Year Milestone of Monolithic Perovskite/Silicon Tandem Solar Cells. *Adv. Mater.* **2024**, *36*, 2311501. [CrossRef]
109. Gao, Q.; Tang, J.; Huang, K.; Kang, X.; Chen, J.; Zhou, X.; Yu, B.-B.; Sheng, Y.; Liu, C. Perovskite Quantum Dots for Improvement in Efficiency of Perovskite Solar Cells: Recent Advances and Prospects. *Adv. Mater. Interfaces* **2025**, *12*, e00587. [CrossRef]
110. Carvalho, D.F.; Conceição, P.M.; Teixeira, J.P.; Salomé, P.M.P.; Fernandes, P.A.; Correia, M.R.P. Modeling and Design Principles for Plasmonic Nanoparticle-Enhanced Perovskite Solar Cells: A Comprehensive Review. *Sol. RRL* **2026**, *10*, e70331. [CrossRef]
111. Winarto, H.; Sutter, J.; Tockhorn, P.; Škorjanc, V.; Patil, P.; Berwig, S.; Zimmermann, L.; Martínez-Denegri, G.; Albrecht, S.; Becker, C. Periodic Inverted Micropyramids for Optically Optimized Fully Textured Solution-Processed Perovskite Solar Cells. *Sol. RRL* **2025**, *9*, e202500613. [CrossRef]
112. Sood, A.K.; Zeller, J.W.; Ghuman, P.; Babu, S.; Soibel, A.; Ting, D.; Gunapala, S.; Chaudhary, L.S.; Efstathiadis, H. Advanced MWIR and LWIR band detection and imaging with nanostructured antireflection coating technology. In *Infrared Sensors, Devices, and Applications XIII*; SPIE: Cergy-Pontoise, France, 2023; Volume 5. [CrossRef]
113. Lamb, D.A.; Irvine, S.J.C.; Clayton, A.J.; Kartopu, G.; Barrioz, V.; Hodgson, S.D.; Baker, M.A.; Grilli, R.; Hall, J.; Underwood, C.I.; et al. Characterization of MOCVD Thin-Film CdTe Photovoltaics on Space-Qualified Cover Glass. *IEEE J. Photovolt.* **2016**, *6*, 557–561. [CrossRef]
114. Zhang, G.; Huang, J.; Wang, L.; Geng, Z.; Zhang, D.; Liu, J. Design and Preparation of Anti-Reflection Nanoarray Structure on the Surface of Space Solar Cell Glass Cover. *Coatings* **2023**, *13*, 1092. [CrossRef]
115. Kang, K.; Byeon, I.; Kim, Y.G.; Choi, J.-R.; Kim, D. Nanostructures in Organic Light-Emitting Diodes: Principles and Recent Advances in the Light Extraction Strategy. *Laser Photonics Rev.* **2024**, *18*, 2400547. [CrossRef]
116. Fusella, M.A.; Saramak, R.; Bushati, R.; Menon, V.M.; Weaver, M.S.; Thompson, N.J.; Brown, J.J. Plasmonic enhancement of stability and brightness in organic light-emitting devices. *Nature* **2020**, *585*, 379–382. [CrossRef]
117. Cui, H.; Teng, C.; Zhao, Y.; Wang, P.; Guo, Y.; Qi, X. Durable self-cleaning antireflective and antifog Al micro-nano structure on glass by laser marker ablation. *Opt. Mater.* **2024**, *147*, 114675. [CrossRef]
118. Li, J.; Ouyang, M.; Wu, J.; Fu, Y.; Ren, H.; Kou, S. Composite bands anti-reflection micro-nano structure surface based on guided mode resonance breaking sub-wavelength conditions. *J. Opt.* **2025**. [CrossRef]

Disclaimer/Publisher's Note: The statements, opinions and data contained in all publications are solely those of the individual author(s) and contributor(s) and not of MDPI and/or the editor(s). MDPI and/or the editor(s) disclaim responsibility for any injury to people or property resulting from any ideas, methods, instructions or products referred to in the content.